Available online at www.sciencedirect.com
ScienceDirect
International Journal of Heat and Mass Transfer 50 (2007) 799–807
International Journal of HEAT and MASS TRANSFER
www.elsevier.com/locate/ijhmt

Numerical study of transient conjugate heat transfer of a turbulent impinging jet

Yue-Tzu Yang *, Shiang-Yi Tsai

Department of Mechanical Engineering, National Cheng Kung University, Tainan 70101, Taiwan, ROC

Received 19 February 2006; received in revised form 25 August 2006
Available online 30 October 2006

Abstract

This study presents the numerical study of transient conjugate heat transfer in a high turbulence air jet impinging over a flat circular disk. The numerical simulation of transient, two-dimensional cylindrical coordinate, turbulent flow and heat transfer is adopted to test the accuracy of the theoretical model. The turbulent governing equations are resolved by the control-volume based finite-difference method with a power-low scheme, and the well-known low-Re κ–ω turbulence model to describe the turbulent structure. The SIMPLE algorithm is adopted to solve the pressure–velocity coupling. The parameters studied include turbulent flow Reynolds number ($Re = 16{,}100$–$29{,}600$), heated temperature of a circular disk ($T_h = 373$ K) or heat flux ($q'' = 63$–189 kW/m^2), and orifice to heat-source spacing ($H/D = 4$–10). The numerical results of the transient impinging process indicate that the jet Reynolds number has a significant effect on the hydrodynamics and heat transfer, particularly in the stagnation region of an impinging jet. High turbulence values lead to greater heat transfer coefficients in the stagnation region and cause a bypass of the laminar-to-turbulent transition region in the wall jet region. Induced turbulence from the environment around the jet also influences the variation of the stagnation heat transfer. The modeling approach used here effectively captures both the stagnation region behavior and the transition to turbulence, thus forming the basis of a reliable turbulence model.

Keywords: Impinging jet; Conjugate heat transfer; Transient; Numerical calculation

1. Introduction

Jet impingement heat transfer has been employed for many industrial applications, e.g., cooling of turbine blades and electrical equipment, drying of paper, textiles, and annealing of metals. Since impinging jets have been widely used in industry fields, extensive research has been conducted to understand the heat transfer characteristics. Improvements on the cooling method are required to avoid unacceptable temperature rise and to maintain a high efficiency. An enhanced heat transfer method such as jet impingement is required to provide the desired thermal environment. Because of the critical requirement of heat transfer uniformity in these applications, it is important to have a turbulence model which can reliably predict local heat transfer rates at every location on the impingement surface. In this study, we further extend the control volume method to calculate the transient conjugate heat transfer of a turbulent impinging jet.

Many investigators presented that three regions characterize the development of the single impinging jet as it flows from the nozzle toward the impingement surface, namely, the free-jet region, the impingement region and the wall jet region. Martin [1] presented extensively to the literature on submerged jet impingement and its heat transfer characteristics by compiling experimental data. Chou and Hung [2] conducted an analytical study for cooling of an isothermal heated surface with a confined slot jet. Chou and Hung [3] performed a numerical study for the fluid flow and heat transfer of slot jet impingement with an extended nozzle.

* Corresponding author. Tel.: +886 6 2757575x62172; fax: +886 6 2352973.
E-mail address: ytyang@mail.ncku.edu.tw (Y.-T. Yang).

0017-9310/$ - see front matter © 2006 Elsevier Ltd. All rights reserved.
doi:10.1016/j.ijheatmasstransfer.2006.08.022

Nomenclature

b	thickness of the disk, m
C_μ, $C_{\omega 1}$, $C_{\omega 2}$	turbulent constant
C	specific heat, kJ/kg K
d	diameter of the disk, m
D	nozzle diameter, m
h	heat transfer coefficient W/m^2 K
H	height of the nozzle from the disk, m
i	turbulence intensity
k	thermal conductivity, W/m K
κ	turbulent kinetic energy, m^2/s^2
P	pressure, kPa
Pr	Prandtl number
q''	wall heat flux, W/m^2
r	radial coordinate, m
Re	Reynolds number, $\frac{V_j D}{\nu}$
t	time, s
T	temperature, K
T_h	heated temperature of circular disk, K
T_{in}	inlet temperature, K
V_j	jet velocity, m/s
V_r	radial velocity, m/s
V_z	vertical velocity, m/s
z	axial coordinate, m

Greek symbols

ρ	density, kg/m^3
μ, μ_t	laminar and turbulent viscosity, N s/m^2
ν	kinematic viscosity, m^2/s
ν_t	turbulent kinetic viscosity N s/m^2
ω	specific dissipation rate of turbulent kinetic energy, m^2/s^2
σ	turbulent constant

Subscripts

f	fluid
s	solid

Seyedein et al. [4] reported the results of numerical simulation of a two-dimensional flow field and heat transfer for a turbulent single-heated slot jet discharging normally into a confined channel. Low and high Re versions of κ–ε turbulence models were used to model the turbulent jet flow. Seyedein et al. [5] demonstrated a numerical simulation for turbulent flow field and heat transfer of three and five turbulent heated slot jets discharging normally into a confined channel. Laschefski et al. [6] numerically analyzed the velocity field and heat transfer in rows of rectangular impinging jets in the transient state. Cziesla et al. [7] simulated turbulent flow issuing from a slot jet array using a subgrid stress model. The numerical study of heat transfer from an impinging jet with $Re = 6500$ and $H/B = 7.22$ was presented by Voke and Gao [8]. It reinforced that the large eddy simulation studies deal with cases having low Reynolds number and a high H/B ratio. In 1998, Yang and Shyu [9] presented numerical predictions on the fluid flow and heat transfer characteristics of multiple impinging slot jets with an inclined confinement surface. The numerical results have shown that the maximum local Nusselt number and maximum pressure on the impinging surface moved downstream while the inclination angle was increased. Sezai and Mohamad [10] presented numerical simulation results for the flow and heat transfer characteristics of an impinging laminar jet issuing from a rectangular slot. The slots of different aspect ratios were studied.

For impinging jets, comparisons between a low Reynolds version of the standard κ–ε with other types of eddy-viscosity models were presented by Behnia et al. [11]. Numerical databases of the impinging jets usually focused on the prediction of heat transfer rates, one or two turbulent models were compared. Papageorgakis and Assanis [12] compared the predictions of incompressible turbulent flows with linear and nonlinear renormalization group (RNG) κ–ε models. It was concluded that combining the claimed universality of the RNG-based κ–ε model constants with the anisotropies introduced by the nonlinear κ–ε model cannot enhance the predictions of both recirculating and shear incompressible flows. Singh et al. [13] developed a finite element model to predict the level of entrainment and mixing in a confined turbulent jet of variable density. Turbulence closure has been achieved by a modified Prandtl mixing length model. The effects of aspect ratio, density ratio, and jet location on entrainment and mixing of ambient fluid were discussed. In 1999, Tzeng et al. [14] employed eight turbulence models including one standard and seven low-Re κ–ε models to predict the heat transfer performance of multiple impinging jets. Validation results indicated that the prediction by each turbulence model depended on grid distribution and numerical scheme used in spatial discretization.

The flowfield induced by a single circular jet exhausting perpendicularly from a flat plate into a crossflow has been investigated numerically by Chochua et al. [15]. An evaluation of the different convection schemes revealed that the second-order upwind scheme did a noticeably better job than the first-order scheme to predict the velocity profile at the jet exit while predicting less mixing than the experimental measurement during the jet and free stream interaction. Rhee and Sung [16] applied the unsteady κ–ε–f_u model and the diffusivity tensor heat transfer model to predict the enhancement of heat transfer in locally forced turbulent separated and reattaching flow over a backward-facing step. The validation of the diffusivity tensor heat transfer model was made by showing the St prediction with

the relevant experiment. More in detail, high and low Reynolds standard κ–ε models were extensively checked by Roy [17].

Chattopadhyay and Saha [18] investigated turbulent flow fields and heat transfer from an array of impinging horizontal knife jets on a moving surface by using large eddy simulation (LES). It has been indicated that increasing surface motion reduced heat transfer for both types of jets. Abdon and Sunden [19] investigated a single round unconfined impinging air jet under different flow and geometrical conditions, to assess the performance of linear and nonlinear two-equation turbulence models. The constitutive relationship of the nonlinear models was shown to be dominated by the linear part of the problem. Concerning the second-order models, some modeling has been made by Shih et al. [20] and showed that second-order models only gave slightly better results than the eddy-viscosity models. Transient conjugate heat transfer during the impingement of a free jet of high Prandtl number fluid on a solid disk of finite thickness was considered by Rahman et al. [21]. The computed results included the velocity, temperature, and pressure distribution in the fluid and the local and average heat transfer coefficient at the solid–fluid interface. The conjugate heat transfer from a discrete heat source to a two-dimensional jet of a high Prandtl number fluid discharging from a slot nozzle was performed by Bula and Rahman [22]. It was found that in addition to jet Reynolds number, plate thickness and its thermal conductivity had a significant impact on temperature distribution and the average Nusselt number.

The numerical investigation of airflow and temperature field in a room with a convective heat source was described by Lu et al. [23]. They concluded that the thermal wall jet created by the heat source greatly influenced airflow pattern and temperature field in the room. The numerical predictions of turbulent plane jets discharged normal to a weak or moderate cross stream were presented by Kalita et al. [24]. The predictions were presented to illustrate the flow pattern involved and to assess the performance of the standard κ–ε model by comparison with available experimental data for three different jets to cross stream velocity ratios and the agreement was found to be satisfactory. A four-equation model was proposed by Mashayek and Taulbee [25] for the prediction of dilute turbulent gas–solid flows where the ratio of the particle and the gas densities was large. These models were used to propose four transport equations for the turbulent kinetic energy of the carrier phase and its rate of dissipation, the turbulence kinetic energy of the dispersed phase, and the velocity covariance of the two phases. The flow and heat transfer characteristics of a turbulent submerged circular air jet impinging on a horizontal flat surface was presented by Siba et al. [26]. An investigation into the predictive performance of linear and nonlinear eddy-viscosity turbulence models for a confined swirling coaxial jet was presented by Yang and Ma [27]. The deficiency in predicting scalar field was perhaps due to the assumption of a constant turbulent Prandtl number and unsteady large-scale motions. Brescianini and Delichatsios [28] tested four high-Re κ–ε turbulence models to assess their suitability in turbulent buoyant jets and plumes. None of the κ–ε models tested can accurately capture all the flow details in both planar and round flows. Jet impingement onto a hole with constant wall temperature was considered by Yilbas et al. [29]. The flow and temperature fields were simulated for a constant standard-off distance, four hole wall temperatures, and two gas jet velocities. It was found that the flow impinging onto the hole spilled from the edges of the hole despite using the same hole and nozzle diameters.

An inverse methodology was used to determine the turbulent component of the heat transfer coefficient in the stagnation region and in the wall-jet region. The effect of nozzle-plate spacing in plane impinging jets using the direct numerical simulation was covered in [30]. It was found that the second peak of the local heat transfer rate (Nusselt number) in the wall jet developing region appeared in the lower nozzle-plate spacing case. Xu and Niu [31] investigated the influences of inlet boundary conditions on the precombustion chamber internal flow patterns, validated by experimental data. For the swirling air flow, inlet boundary condition specifications, two methods are compared employing the standard κ–ε turbulence model. The simulation indicated that proper inlet conditions were essential in the case of a swirling inlet, although there remained some discrepancies between the simulation results and the experimental data. The detailed flow field characteristics of a turbulent air slot jet impinging on a semicircular convex surface was investigated numerically by Yang and Hwang [32]. This study was useful in helping researchers to understand the flow field characteristics in the stagnation regions of impingement surfaces. A new algebraic turbulent mass flux model has been proposed and formulated by Wei et al. [33]. The turbulent mixing between the swirling air flow and the helium/air jet in a combustor have been simulated numerically. The gas axial and tangential velocities, as well as the gas axial and tangential fluctuating velocities predicted by the new ASM/κ–ε model, agreed with the measurements. In 2004, the development of a new subgrid-based wall function has been presented by Craft et al. [34], the boundary-layer-type transport equations were solved locally across an embedded grid within the near-wall cell. It has been shown that the new wall function achieved an excellent agreement with results obtained using low-Re models, while requiring only a modest increased in computing time compared with a standard wall function.

Three-dimensional numerical simulations of fluid flow and heat transfer characteristics for an inclined jet with crossflow impinging on a heating plate was presented by Yang and Wang [35]. The generation of a pair of counter-rotating longitudinal vortices was clearly observed from the computations. The flow and heat transfer in two planar impinging jets using large-eddy simulation and experiments were demonstrated by Akiyama et al. [36]. For both the

unforced and forced flows the large-eddy simulation predictions have shown that the jet develops streamwise vorticity, and the turbulent inflow condition provided disturbances that the jets can be efficiently amplified. Chen et al. [37] provided detailed theoretical solutions on laminar flow for free-surface slot jet impinging onto horizontal surfaces under arbitrary-heat-flux conditions. The thermal and hydraulic boundary layers of laminar flow were divided into four regions of flow along heat transfer surfaces including a stagnation zone and three wall jet zones. Numerical predictions of heat transfer coefficients under jet impingement from an array of nozzles have been made by Salamah and Kaminski [38]. A study of the capabilities of several turbulence models to capture the physical characteristics of a single round nozzle and a single slot nozzle jets was conducted by Coussirat et al. [39]. Computations confirmed that velocity fluctuations were not adequately predicted at the stagnation zone, and their values strongly depended on the turbulence model used. Shi et al. [40] developed a new Eulerian–Lagrangian model to predict the heat transfer in multiple-turbulent-slot impinging jets of dilute gas-particle suspensions by taking into account the conduction heat transfer due to particle-wall collisions. It was shown that with inclusion of the conduction heat transfer, the numerical results compared favorably with the available experimental results. El-Gabry and Kaminski [41] used the computational fluid dynamics models to predict the heat transfer distribution on a smooth surface under an array of angled impinging jets. Two turbulence models were examined, the standard κ–ε model and the Yang–Shih model. The Yang–Shih model, though it overpredicted peak Nusselt numbers (more so than the standard κ–ε model), was more effective in predicting heat transfer between jets. An algorithm for calculating the flame structure of lifted jet fires has been presented by Cumber and Spearpoint [42]. The algorithm was based on an extension of a fire model used to simulate rim-stabilized flames. It was found that the radiation heat flux distributions in the far field were insensitive to the lift-off model implemented, consistent with the prediction of the mean temperature field calculated using each lift-off model. Navaratnam et al. [43] investigated numerically the transient behavior of a single, two-dimensional synthetic jet. A novel moving-grid methodology has been used to model the synthetic jet in crossflow. Over the last few years, CFD using Reynolds-averaged Navier–Stokes equations, coupled with turbulence modeling has become a standard practical simulation tool for the design and analysis of engineering systems. The objective of the present study is to provide a physical insight into conjugate heat transfer effects and to facilitate the validation of numerical conjugate heat transfer models.

2. Mathematical formulation

Consider an axial jet discharged from a circular nozzle and impinged on a uniformly heated solid disk as shown in Fig. 1. The following assumptions are made to model the conjugate heat transfer problem:

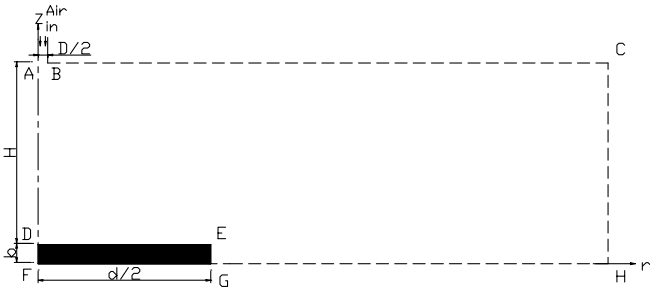

Fig. 1. Physical coordinate system and boundary conditions.

(1) unsteady,
(2) incompressible fluid,
(3) turbulent axisymmetric,
(4) constant fluid properties, and
(5) negligible radiative and natural convective heat transfer.

The governing equations of mass, momentum, turbulent kinetic energy, specific turbulent energy dissipation rate, and energy in the transient turbulent flow using the low Reynolds number κ–ω model can be written as

Continuity equation:

$$\frac{\partial(\rho u_i)}{\partial x_i} = 0 \tag{1}$$

Momentum equation:

$$\frac{\partial(\rho u_i)}{\partial t} + \rho u_j \frac{\partial u_i}{\partial x_i} = -\frac{\partial p}{\partial x_i} + \frac{\partial}{\partial x_j}\left[\mu_t\left(\frac{\partial u_i}{\partial x_j} + \frac{\partial u_j}{\partial x_i}\right)\right] \tag{2}$$

Turbulent kinetic energy equation:

$$\frac{\partial(\rho\kappa)}{\partial t} + \frac{\partial(\rho u_j \kappa)}{\partial x_j} = \rho P - \rho\omega\kappa + \frac{\partial}{\partial x_j}\left[\left(\mu + \frac{\mu_t}{\sigma_\kappa}\right)\frac{\partial\kappa}{\partial x_j}\right] \tag{3}$$

where $\mu_t = \rho C_\mu \frac{\kappa}{\omega}$ and the production term P is defined as

$$P = \nu_t\left[\frac{\partial u_i}{\partial x_j} + \frac{\partial u_j}{\partial x_i} - \frac{2}{3}\frac{\partial u_m}{\partial x_m}\delta_{ij}\right]\frac{\partial u_i}{\partial x_j} - \frac{2}{3}\kappa\frac{\partial u_m}{\partial x_m}$$

Specific dissipation rate of turbulent kinetic energy:

$$\frac{\partial(\rho\omega)}{\partial t} + \frac{\partial(\rho u_j \omega)}{\partial x_j} = C_{\omega 1}\rho P\omega - C_{\omega 2}\rho\omega^2 + \frac{\partial}{\partial x_j}\left[\left(\mu + \frac{\mu_t}{\sigma_\omega}\right)\frac{\partial\omega}{\partial x_j}\right] \tag{4}$$

Energy equation of fluid:

$$\frac{\partial(\rho T)}{\partial t} + \rho u_j \frac{\partial T}{\partial x_j} = \frac{\partial}{\partial x_j}\left[\left(\frac{\mu}{Pr} + \frac{\mu_t}{\sigma_T}\right)\frac{\partial T}{\partial x_j}\right] \tag{5}$$

The empirical constants appear in the above equations are given by the following values: $C_\mu = 0.09$, $C_{\omega 1} = 0.555$, $C_{\omega 2} = 0.833$, $\sigma_\kappa = 2.0$, $\sigma_\omega = 2.0$ and $\sigma_T = 1.0$.

The equation describing the conservation of energy for solid can be written as follows:

$$\frac{\partial(\rho_s C T_s)}{\partial t} = \frac{\partial\left(k_s \frac{\partial T_s}{\partial x_i}\right)}{\partial x_i} \tag{6}$$

As the time $t > 0$, the boundary conditions adopted in the present study are written as follows:

(1) Inlet boundary (A–B)

$$V_r = 0, \quad V_z = -V_j$$
$$T_{in} = 298\ \mathrm{K}$$
$$\kappa = \kappa_{in} = \frac{3}{2}(iV_j^2), \text{ where } i \text{ is the turbulence intensity}$$
$$\omega = \omega_{in} = \frac{\kappa}{v_t}, \quad v_t = 0.01v$$

(2) Axisymmetric boundary (A–D)

$$V_r = 0, \quad \frac{\partial V_z}{\partial r} = 0$$
$$\frac{\partial \kappa}{\partial r} = \frac{\partial \omega}{\partial r} = \frac{\partial T}{\partial r} = 0$$

(3) Entrainment boundary (B–C), (C–H), (G–H)

$$p = p_{atm}, \quad T = 25\,^{\circ}C, \quad \frac{\partial \kappa}{\partial r} = 0, \quad \frac{\partial \omega}{\partial r} = 0 \text{ (exit)}$$
$$p = p_{atm}, \quad T = 25\,^{\circ}C, \quad \frac{\partial \kappa}{\partial z} = 0, \quad \frac{\partial \omega}{\partial z} = 0 \text{ (top wall)}$$

(4) Conjugated boundary (D–E)

$$T_f = T_s$$
$$V_r = V_z = 0$$
$$k_s \frac{\partial T_s}{\partial z} = k_f \frac{\partial T_f}{\partial z}$$
$$\kappa = 0, \quad \omega = 0$$

(5) Constant temperature or constant heat flux boundary (F–G)

$$T_s = T_h \quad \text{or} \quad -k_s \frac{\partial T_s}{\partial z} = q''$$

(6) Adiabatic boundary (D–F), (E–G)

$$V_r = V_z = 0$$
$$\kappa = 0, \quad \omega = 0$$
$$\frac{\partial T_s}{\partial r} = 0$$

The disk and the fluid are assumed to be in an equilibrium isothermal condition at the start of the transient heating process. A complementary time step independencies study was performed for the unsteady flows.

3. Numerical computation

The numerical computations were carried out by solving the governing conservation equations with the boundary conditions. A non-uniform grid system with a large concentration of nodes in the regions of steep gradients was employed. The numerical method used in the present study is based on the SIMPLE algorithm of Patankar [44]. This is an iterative solution procedure where the computation is begun by guessing the pressure field. The momentum equation is solved to determine the velocity components. Even though the continuity equation does not contain any pressure, it can be transformed easily into a pressure correction equation. The conservation equations are discretized by a control volume-based finite difference method with a power-law scheme. The set of difference equations are solved iteratively using a line-by-line solution method in conjunction with a tridiagonal matrix form. The solution is considered to be converged when the normalized residual of the algebraic equation is less than a prescribed value of 10^{-4}. For the validation of the theoretical model and the choice of appropriate boundary conditions, the numerical results are compared to the available experimental results in the literature for $H/D = 10$, $Re = 16{,}100$, shown in Fig. 2. It indicates that the stagnation region heat transfer coefficient is relatively high compared to that of the wall jet region. Turbulence levels at the nozzle exit play a key role on the stagnation point heat transfer and in the wall jet regions. High turbulence values lead to greater heat transfer coefficients in the stagnation region and cause a bypass of the laminar-to-turbulent transition region in the wall jet region. Induced turbulence from the environment around the jet also influences the variation of the stagnation heat transfer with nozzle height above the disk. A comparison of theoretical predictions with the experimental data in the literature was used to assess the grid independence of the results. Different size meshes, 41×126, 51×136 and 61×146 in r-, and z-directions, respectively, were employed in testing the numerical model. It has been validated using experimental data reported in Siba et al. [26]. Certain discrepancies between calculations and the available data of Siba et al. [26] may be caused by the roundoff and discretization or measurement errors. In addition, the three dimensionality of the flow due to secondary vortices in jet generation apparatus may contribute to the discrep-

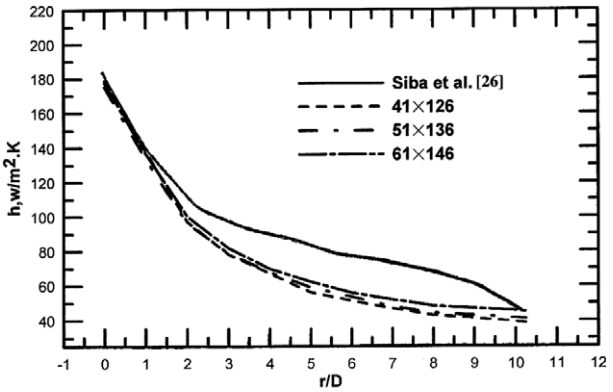

Fig. 2. Effect of grid refinement on heat transfer coefficient.

ancy between model predictions and experimental data. Considering these factors, the overall comparison with test data is satisfactory. These computations performed on IBM-RS6000F50, took about 18,000–25,200 s CPU time.

4. Results and discussion

The numerical algorithm and computer program were carefully evaluated by comparing model predictions with available experimental data in the literature. The velocity vectors of a turbulent axisymmetric air jet for $Re = 29{,}600$, $t = 30$ s and $H/D = 4$–10 are shown in Fig. 3. Since the diameter is large compared to that of the jet exit diameter, the flow field is divided into three regions: free jet region, impingement region and the wall jet region. The free jet region develops from the exit of the nozzle and becomes turbulent. The impingement or stagnation region, where the strong interaction of the jet with the surface produces a deceleration as it approaches the surface. The flow then changes its direction and starts accelerating away

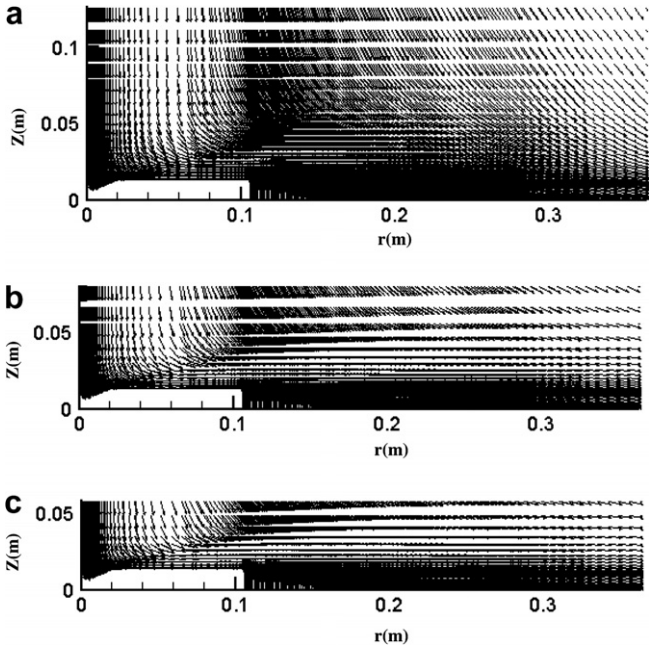

Fig. 3. Velocity vector for $Re = 29{,}600$, $t = 30$ s. (a) $H/D = 10$, (b) $H/D = 6$, (c) $H/D = 4$.

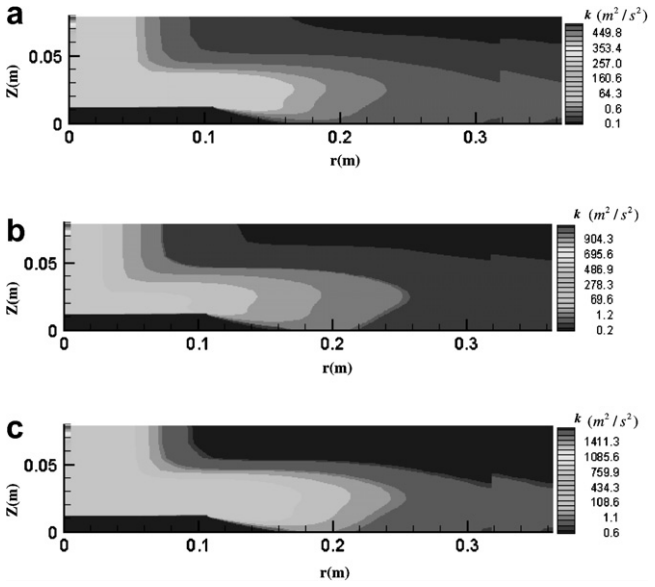

Fig. 4. Turbulent kinetic energy contour for $H/D = 6$, $T_h = 373$ K and $t = 30$ s. (a) $Re = 16{,}100$, (b) $Re = 23{,}700$, (c) $Re = 29{,}600$.

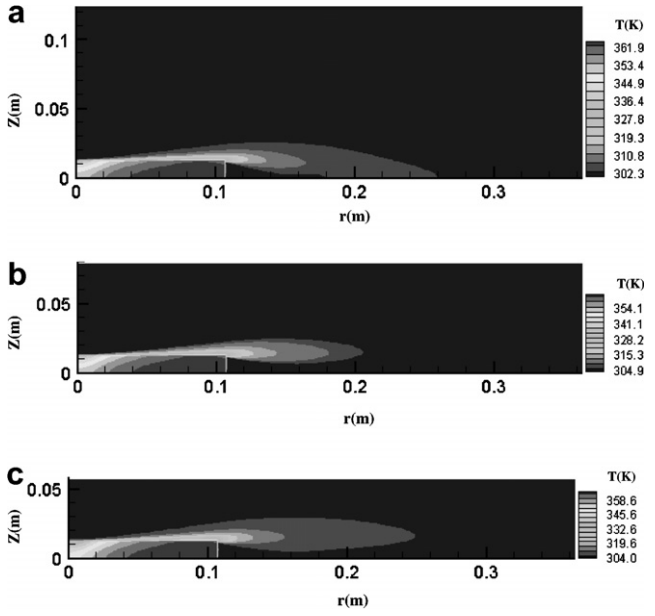

Fig. 5. Temperature contour for $Re = 16{,}100$, $T_h = 373$ K and $t = 30$ s. (a) $H/D = 10$, (b) $H/D = 6$, (c) $H/D = 4$.

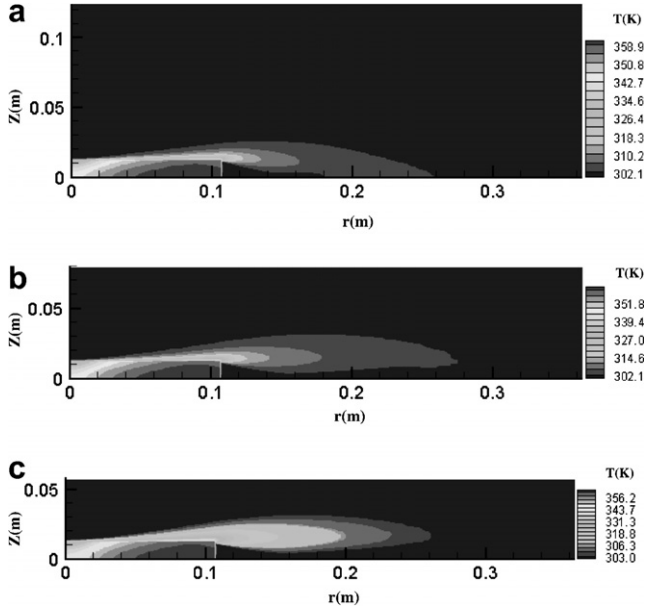

Fig. 6. Temperature contour for $Re = 23{,}700$, $T_h = 373$ K and $t = 30$ s. (a) $H/D = 10$, (b) $H/D = 6$, (c) $H/D = 4$.

from the stagnation point. The wall jet region where the flow leaving the stagnation region begins to decelerate in a direction parallel to the targeted test surface. Fig. 4 presents the turbulent kinetic energy counter for different Reynolds number at $H/D = 6$, $Re = 16{,}100$, 23,700 and 29,600. The fields of the turbulent kinetic energy are similar. The highest values of the turbulent kinetic energy are on the top of the disk and the shear layer.

The contours of transient temperature are shown in Figs. 5 and 6 for $T_h = 373$ K, $H/D = 4$, 6 and 10, $Re =$ 16,100 and 23,700. Note that at the early stages of the heat transfer process, the temperature at the interface rises uniformly at all locations, resulting in a practically isothermal interface condition. The thickness of the boundary layer increases with time and becomes significant only in the latter part of the transient. Because the leading edge of the boundary layer is located at the stagnation point and its thickness increases downstream, it can be seen that the transient temperature reaches a minimum at the impinging point and a maximum at the outer edge of the disk. A better cooling can be achieved by setting $H/D = 4$ for the same Reynolds number. Fig. 7 presents the transient temperature contour for $T_h = 373$ K, $Re = 23{,}700$ and $H/D = 10$. A high temperature is seen at the stagnation region because the cold fluid from the jet strikes at that location and main-

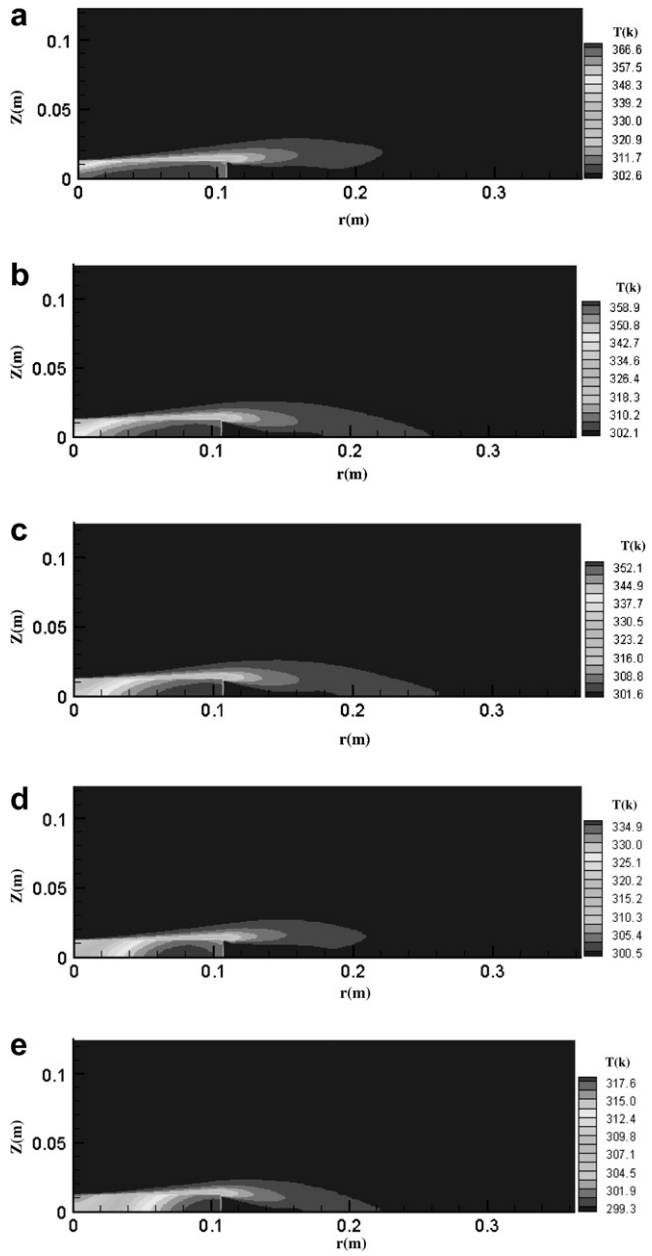

Fig. 7. Transient temperature contour for $Re = 23{,}700$, $H/D = 10$, $T_h = 373$ K. (a) $t = 10$ s, (b) $t = 30$ s, (c) $t = 50$ s, (d) $t = 100$ s, (e) $t = 200$ s.

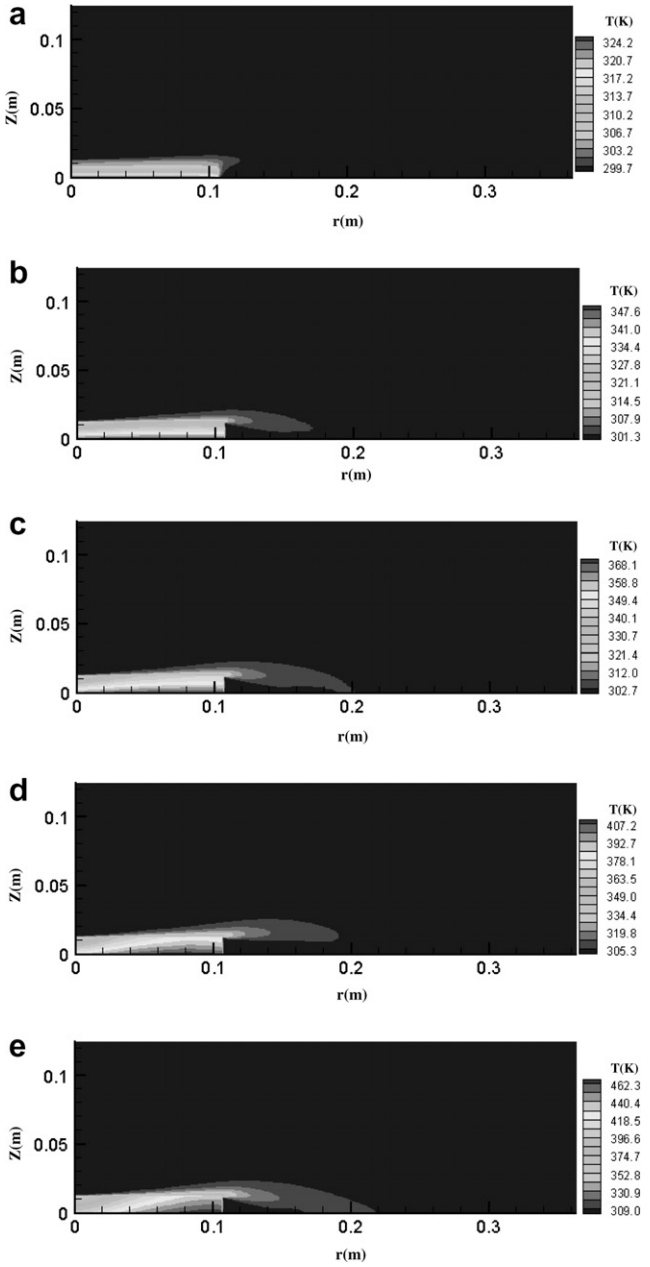

Fig. 8. Transient temperature contour for $Re = 23{,}700$, $H/D = 10$, $q'' = 63$ kW/m^2. (a) $t = 10$ s, (b) $t = 30$ s, (c) $t = 50$ s, (d) $t = 100$ s, (e) $t = 200$ s.

tains the minimum temperature at the interface. The heat transfer at that location is the highest because of the constant renewal of cold fluid in order to carry away the heat. For $t > 200$ s it will reach a steady-state. In Fig. 8, the transient temperature contour for $q'' = 63\ \mathrm{kW/m^2}$, $Re = 23{,}700$ and $H/D = 10$ is shown for different thermal boundaries. As expected, the temperature increases with time starting from the initial condition, a rapid increment is seen at the earlier part of the transient. Note that the time required to reach a steady-state condition is lower at the higher Reynolds number because a higher velocity of fluid helps to enhance the convective heat transfer process. As temperature rises with time, the thermal storage in the solid decreases and more heat proceeds to the interface and dissipates to the fluid. The interfacial heat flux increases rapidly with time in the earlier part of the transient and increases slowly as the steady-state condition is approached. Fig. 9 shows the computed surface temperature data to illustrate the behavior of the impinging jet for $Re = 23{,}700$, $H/D = 10$ and $T_h = 373$ K. As the time progresses, the surface temperature decreases steeply at any radial position especially in the stagnation region. The surface temperature distribution at different heat fluxes for $Re = 29{,}600$, $H/D = 10$ and $t = 50$ s is presented in Fig. 10. It shows the solid–fluid interface temperature distribution for different heat fluxes. It can be observed that the minimum temperature is present at the stagnation point and the maximum is at the edge of the disk. As expected, the interface temperature, as well as the minimum-to-maximum surface temperature differs as the interface increases with heat flux.

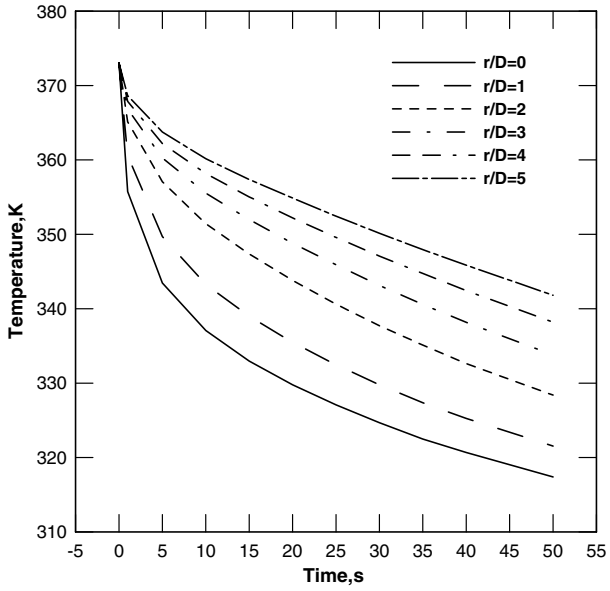

Fig. 9. Surface temperature distribution at different r/D locations for $Re = 23{,}700$, $H/D = 10$, and $T_h = 373$ K.

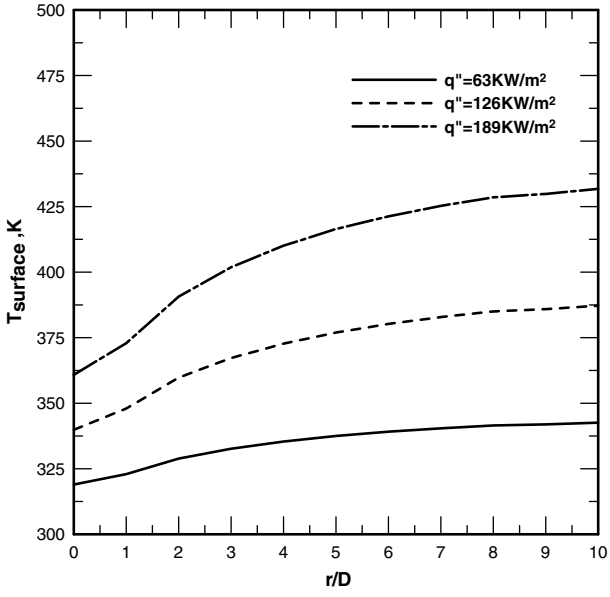

Fig. 10. Surface temperature distribution at different heat flux for $Re = 29{,}600$, $H/D = 10$, and $t = 50$ s.

5. Conclusions

Transient conjugate heat transfer in a high turbulence air jet impinging over a flat circular disk is investigated numerically with the finite-difference algorithm SIMPLE. This study focuses on the turbulent regime using the low-Re κ–ω turbulence model. The jet Reynolds number was found to be an important parameter controlling the transient process. Computational results show that heat transfer is maximum at the stagnation point and decreases with distance along the disk. The time required to reach the steady-state condition decreases as the Reynolds number increases. The numerical predictions obtained from this study provide a detailed insight into the conjugate heat transfer effects and facilitate the validation of numerical conjugate heat transfer models.

Acknowledgements

We would like to thank the National Science Council of the Republic of China for supporting this project under contract No. NSC 93-2212-E-006-046. The use of compute resources provided by the National Center for High-Performance Computing is gratefully acknowledged.

References

[1] H. Martin, Heat and mass transfer between impinging gas jets and solid surfaces, Adv. Heat Transfer 13 (1977) 1–60.
[2] Y.J. Chou, Y.H. Hung, Impingement cooling of an isothermally heated surface with a confined slot jet, ASME, J. Heat Transfer 116 (1994) 479–482.
[3] Y.J. Chou, Y.H. Hung, Fluid flow and heat transfer of an extended slot jet impingement, J. Thermophys. Heat Transfer 8 (1994) 538–545.
[4] S.H. Seyedein, M. Hasan, A.S. Mujumdar, Modeling of a single confined turbulent slot jet impingement using various κ–ε turbulence models, Appl. Math. Model. 18 (1994) 526–537.

[5] S.H. Seyedein, M. Hasan, A.S. Mujumdar, Turbulent flow and heat transfer from confined multiple impinging slot jets, Numer. Heat Transfer 27 (1995) 35–51.
[6] H. Laschefski, T. Cziesla, G. Biswas, N.K. Mitra, Numerical investigation of heat transfer by rows of rectangular impinging jets, Numer. Heat Transfer 30 (1996) 87–101.
[7] T. Cziesla, E. Tandogan, N.K. Mitra, Large eddy simulations of heat transfer from impinging slot jets, Numer. Heat Transfer 32 (1997) 1–17.
[8] P. Voke, S. Gao, Numerical study of heat transfer from impinging jet, Int. J. Heat Mass Transfer 141 (1998) 671–680.
[9] Y.T. Yang, C.H. Shyu, Numerical study of multiple impinging slot jets with an inclined confinement surface, Numer. Heat Transfer 33 (1998) 23–37.
[10] I. Sezai, A.A. Mohamad, Three-dimensional simulation of laminar rectangular impinging jets, ASME J. Heat Transfer 121 (1999) 50–56.
[11] P. Behnia, S. Parneix, Y. Shabany, P. Durbin, Numerical study of turbulent heat transfer in confined and unconfined impinging jets, Int. J. Heat Fluid Flow 20 (1999) 1–9.
[12] G.C. Papageorgakis, D.N. Assanis, Comparison of linear and nonlinear RNG-based κ–ε models for incompressible turbulent flows, Numer. Heat Transfer 35 (1999) 1–22.
[13] G. Singh, T. Sundararajan, U.S.P. Shet, Entrainment and mixing studies for a variable density confined jet, Numer. Heat Transfer 35 (1999) 205–223.
[14] P.Y. Tzeng, C.Y. Soong, C.D. Hsieh, Numerical investigation of heat transfer under confined impinging turbulent slot jets, Numer. Heat Transfer 35 (1999) 903–924.
[15] G. Chochua, W. Shyy, S. Thakur, A. Brankovic, J. Lienau, L. Porter, D. Lischinsky, A computational and experimental investigation of turbulent jet and crossflow interaction, Numer. Heat Transfer 38 (2000) 557–572.
[16] G.H. Rhee, H.J. Sung, Enhancement of heat transfer in turbulent separated and reattaching flow by local forcing, Numer. Heat Transfer 37 (2000) 733–753.
[17] S. Roy, Numerical investigation of the blade cooling effect generated by multiple jets issuing at an angle into a incompressible horizontal crossflow, Numer. Heat Transfer 38 (2000) 701–718.
[18] H. Chattopadhyay, S.K. Saha, Numerical investigation of heat transfer over a moving surface due to impinging knife-jets, Numer. Heat Transfer 39 (2001) 531–549.
[19] A. Abdon, B. Sunden, Numerical investigation of impingement heat transfer using linear and nonlinear two-equation turbulence models, Numer. Heat Transfer 40 (2001) 563–578.
[20] Y. Shih, M. Ray, S. Mujemdar, Computational study of impingement heat transfer under a turbulent slot jet, Ind. Eng. Chem. Res. 41 (2002) 4643–4651.
[21] Muhammad M. Rahman, Antonio J. Bula, John E. Leland, Analysis of transient conjugate heat transfer to a free impinging jet, J. Thermophys. Heat Transfer 14 (2000) 330–339.
[22] Antonio J. Bula, Muhammad M. Rahman, Numerical modeling of conjugate heat transfer during impingement of free liquid jet issuing from a slot nozzle, Numer. Heat Transfer 38 (2000) 45–66.
[23] W.Z. Lu, C.M. Tam, A.Y.T. Leung, A.T. Howarth, Numerical investigation of convective heat transfer in a heated room, Numer. Heat Transfer 42 (2002) 233–251.
[24] K. Kalita, A. Dewan, A.K. Dass, Prediction of turbulent plane jet in crossflow, Numer. Heat Transfer 41 (2002) 101–111.
[25] F. Mashayek, D.B. Taulbee, A four-equation model for prediction of gas–solid turbulent flows, Numer. Heat Transfer 41 (2002) 95–116.
[26] Erick A. Siba, M. Ganesa-Pillai, Kendall T. Harris, A. Haji-Sheikh, Heat transfer in a high turbulence air jet impinging over a flat circular disk, ASME J. Heat Transfer 125 (2003) 257–265.
[27] X. Yang, H. Ma, Linear and nonlinear eddy-viscosity turbulence models for a confined swirling coaxial jet, Numer. Heat Transfer 43 (2003) 289–305.
[28] C.P. Brescianini, M.A. Delichatsios, New evaluation of the κ–ε turbulence model for free buoyant plumes, Numer. Heat Transfer 43 (2003) 731–751.
[29] B.S. Yilbas, S.Z. Shuja, M.Q. Budair, Jet impingement onto a hole with constant wall temperature, Numer. Heat Transfer 43 (2003) 843–865.
[30] Hirofumi Hattori, Yasutaka Nagano, Direct numerical simulation of turbulent heat transfer in a plane impinging jet, Int. J. Heat Fluid Flow 25 (2004) 749–758.
[31] H.T. Xu, J.L. Niu, Numerical simulation and experimental validation of the swirling turbulent air flow and mixing processes, Numer. Heat Transfer 46 (2004) 571–586.
[32] Y.T. Yang, C.H. Hwang, Numerical simulations on the hydrodynamics of a turbulent slot jet impinging on a semicylindrical convex surface, Numer. Heat Transfer 46 (2004) 995–1008.
[33] X. Wei, J. Zhang, L. Zhou, A new algebraic mass flux model for simulating turbulent mixing in swirling flow, Numer. Heat Transfer 45 (2004) 283–300.
[34] T.J. Craft, S.E. Gant, H. Iacovides, B.E. Launder, A new wall function strategy for complex turbulent flows, Numer. Heat Transfer 45 (2004) 301–318.
[35] Y.T. Yang, Y. X Wang, Three-dimensional numerical simulation of an inclined jet with cross-flow, Int. J. Heat Mass Transfer 48 (2005) 4019–4027.
[36] T. Akiyama, K. Yamamoto, K.D. Squires, K. Hishida, Simulation and measurement of flow and heat transfer in two planar impinging jets, Int. J. Heat Fluid Flow 26 (2005) 244–255.
[37] Y.C. Chen, C.F. Ma, M. Qin, Y.X. Li, Theoretical study on impingement heat transfer with single-phase free-surface slot jets, Int. J. Heat Mass Transfer 48 (2005) 3381–3386.
[38] Samir A. Salamah, Deborah A. Kaminski, Modeling of turbulent heat transfer from an array of submerged jets impinging on a solid surface, Numer. Heat Transfer 48 (2005) 315–337.
[39] M. Coussirat, J. van Beeck, M. Mestres, E. Egusguiza, J.M. Buchlin, X. Escaler, Computational fluid dynamics modeling of impinging gas-jet systems: I. Assessment of eddy viscosity models, ASME J. Fluids Eng. 127 (2005) 691–703.
[40] Y.L. Shi, A.S. Mujumdar, M.B. Ray, Heat transfer in multiple-turbulent-slot impinging jets of gas-particle suspensions, Numer. Heat Transfer 47 (2005) 147–164.
[41] L.A. El-Gabry, D.A. Kaminski, Numerical investigation of jet impingement with cross flow-comparison of Yang–Shih and standard κ–ε turbulence models, Numer. Heat Transfer 47 (2005) 441–469.
[42] P.S. Cumber, M. Spearpoint, Modeling lifted methane jet fires using the boundary-layer equations, Numer. Heat Transfer 49 (2006) 239–258.
[43] K. Navaratnam, Dong-Dae Lee, Siva Parameswaran, Application of a novel moving-grid methodology to model the internation of a synthetic jet with a turbulent boundary layer, Numer. Heat Transfer 49 (2006) 105–123.
[44] S.V. Patankar, Numerical Heat Transfer and Fluid Flow, McGraw-Hill, New York, 1980.